Smooth muscle–endothelial cell communication activates Reelin signaling and regulates lymphatic vessel formation

Sophie Lutter, Sherry Xie, Florence Tatin, and Taija Makinen

Lymphatic Development Laboratory, Cancer Research UK London Research Institute, London WC2A 3LY, England, UK

Active lymph transport relies on smooth muscle cell (SMC) contractions around collecting lymphatic vessels, yet regulation of lymphatic vessel wall assembly and lymphatic pumping are poorly understood. Here, we identify Reelin, an extracellular matrix glycoprotein previously implicated in central nervous system development, as an important regulator of lymphatic vascular development. Reelin-deficient mice showed abnormal collecting lymphatic vessels, characterized by a reduced number of SMCs, abnormal expression of lymphatic capillary marker lymphatic vessel endothelial hyaluronan receptor 1 (LYVE-1), and impaired function. Furthermore, we show that SMC recruitment to lymphatic vessels stimulated release and proteolytic processing of endothelium-derived Reelin. Lymphatic endothelial cells in turn responded to Reelin by up-regulating monocyte chemotactic protein 1 (MCP1) expression, which suggests an autocrine mechanism for Reelin-mediated control of endothelial factor expression upstream of SMC recruitment. These results uncover a mechanism by which Reelin signaling is activated by communication between the two cell types of the collecting lymphatic vessels—smooth muscle and endothelial cells—and highlight a hitherto unrecognized and important function for SMCs in lymphatic vessel morphogenesis and function.

Introduction

The lymphatic vasculature initially develops as a primitive plexus of identical vessels, all expressing the hyaluronan receptor lymphatic vessel endothelial hyaluronan receptor 1 (LYVE-1). This plexus is extensively remodeled to give rise to the functional lymphatic vasculature, which consists of two distinct vessel types: lymphatic capillaries (also called initial lymphatics) and collecting lymphatic vessels (Jurisic and Detmar, 2009; Tammela and Alitalo, 2010). Only blind-ended lymphatic capillaries retain expression of LYVE-1, and their distinctive morphology is ideally suited to their function; loose, overlapping cell–cell junctions, discontinuous basement membrane (BM), and wide lumens allow efficient absorption of protein-rich fluid from the interstitium. The fluid is further drained into the collecting lymphatic vessels, which develop luminal valves and a BM, and recruit smooth muscle cells (SMC), to assist in the unidirectional propulsion of lymph (Jurisic and Detmar, 2009; Tammela and Alitalo, 2010).

In the blood vessels, the vascular BM is an important structural component, which is formed predominantly of Collagen IV, laminin, nidogen/entactin, and heparan sulfate proteoglycans (Sasaki et al., 2004). It helps to keep the vessel wall structure in shape and withstand mechanical forces generated by pulsatile blood flow and vasoconstriction, which regulates blood flow and pressure. In addition to its structural importance, more recent studies have revealed a complex functionality of the vascular BM, including involvement in endothelial cell (EC) migration, proliferation, survival, signal transduction, and vessel morphogenesis (Aszódi et al., 2006). In addition, because the vascular BM is produced by and shared between ECs and SMCs, it directly interacts with both cell types to modulate their behavior and communication. For example,

Correspondence to Taija Makinen: taija.makinen@cancer.org.uk

Abbreviations used in this paper: α-SMA, α-smooth muscle actin; BEC, blood vascular endothelial cell; BM, basement membrane; EC, endothelial cell; HAoSMC, human aortic smooth muscle cell; HUVSMC, human umbilical venous smooth muscle cell; ICG, indocyanine green; LEC, lymphatic EC; LYVE-1, lymphatic vessel endothelial hyaluronan receptor 1; MCP1, monocyte chemotactic protein 1; PECAM-1, platelet EC adhesion molecule 1; qPCR, quantitative PCR; SMC, smooth muscle cell; TSA, tyramide signal amplification.

The Rockefeller University Press $30.00
J. Cell Biol. Vol. 197 No. 6 837–849
www.jcb.org/cgi/doi/10.1083/jcb.201110132

endothelial-derived ECM can stimulate proliferation of SMC in vitro (Figueroa et al., 2004). Similarly, Heparan-sulfate (HS), deposited by ECs, can support mural cell attachment on the vessels in vivo; however, the mural cells require cell-autonomous HS to efficiently polarize and migrate to the nascent blood vessels (Stenzel et al., 2009). ECM molecules can also participate in storing, masking, presenting, or sequestering growth factors, thereby modulating their bioavailability and activity (Hynes, 2009). Furthermore, during development, the vascular BMs undergo compositional and structural alterations, including conformational changes and proteolytic processing of specific matrix components, which can provide important angiogenic or anti-angiogenic cues (for review see Kalluri, 2003).

In contrast to the vascular BM, little is known of the composition and importance of the ECM of lymphatic vessels. Here, we identify Reelin as a lymphatic-specific matrix molecule and demonstrate its important function in the formation of functional collecting lymphatic vessels. In addition, we uncover a unique mechanism by which Reelin signaling is activated via communication between the two cell types that form the collecting vessels: endothelial and SMCs. The specific defects displayed by the *Reln*-deficient mice further highlight a hitherto unrecognized important function of SMCs in lymphatic vessel morphogenesis and function.

Results

Characterization of collecting vessel formation and lymphatic vascular wall assembly

To establish a timeline and a defined set of markers of lymphatic collecting vessel differentiation, we investigated SMC recruitment to dermal lymphatic vessels using antibodies against α-smooth muscle actin (α-SMA), desmin, and NG2, the markers of SMCs and pericytes; and against LYVE-1, a marker of immature lymphatic vessels and lymphatic capillaries. The developing vasculature was analyzed in mouse ear skin, which allows whole-mount visualization of vessels that grow postnatally into the ear to form a primary vascular plexus, which is subsequently remodeled into a functional vessel network consisting of lymphatic capillaries and collecting vessels (Mäkinen et al., 2005). During the first postnatal week, the expanding dermal lymphatic vasculature of the ear was devoid of SMCs and the endothelia was uniformly positive for LYVE-1 (unpublished data). At postnatal day 12 (P12), LYVE-1 was down-regulated in specific areas (Fig. 1 A). Although the first α-SMA–positive SMCs could be found loosely attached to the lymphatic vessels at this stage, LYVE-1 down-regulation did not correlate with their presence (Fig. 1 A and not depicted). At P14, developing collecting vessels acquired SMCs, which were found predominantly in areas of low LYVE-1 expression (Fig. 1 B). By P16, lymphatic collecting vessels were identified by their prominent SMC coverage and absent LYVE-1 expression (Fig. 1 C). NG2, a marker of vascular pericytes, was not expressed in lymphatic SMCs (Fig. 1 D), whereas desmin-positive SMCs were found only in lymphatic vessels that had acquired features of mature collecting vessels, such as prominent SMC coverage, luminal valves, and complete down-regulation of LYVE-1 expression (Fig. 1, E–G). Desmin and α-SMA were coexpressed in lymphatic SMCs (Fig. 1 H).

Another characteristic feature of collecting lymphatic vessels is the presence of vascular BM. To investigate if matrix deposition can serve as a marker of collecting vessel differentiation, we examined the expression of Collagen IV and Laminin-α5 in the developing vessels. At P14, Collagen IV was evident in LYVE-1–positive vessels that had no SMCs (Fig. 1, I and I′), which suggests its deposition by ECs. At later stages, Collagen IV was found predominantly around collecting vessels (Fig. 1, J and J′), with lower levels in capillaries (not depicted; Pflicke and Sixt, 2009). Conversely, Laminin-α5 expression was not detectable in prospective collecting lymphatic vessels before SMC recruitment, except in luminal valves (Fig. 1, K and K′; Bazigou et al., 2009). In more matured collecting vessels, Laminin-α5 staining highlighted the SMCs around collecting vessels (Fig. 1, L and L′), which suggests that these cells are its main source. However, in the blood vasculature, Laminin-α5 is produced by ECs (Wu et al., 2009), and additional expression by lymphatic endothelium that may be induced upon SMC contact cannot be excluded. In summary, these results suggest that both endothelial and SMCs contribute to the production of matrix components of the lymphatic BM. In addition, deposition of ECM may provide the earliest sign of collecting vessel specification (Fig. 1 M).

Identification of Reelin as a lymphatic endothelial-specific matrix molecule

To further characterize lymphatic vessel wall assembly, we attempted to identify new specific components of the lymphatic BM. We dissected mesenteric collecting lymphatic vessels, arteries, and veins of P7 mice and identified differentially expressed genes using Affymetrix expression arrays. The reliability of the dataset was demonstrated by the identification of several known lymphatic, arterial, and venous markers that were up- or down-regulated in the appropriate datasets (Table S1). 14 genes involved in ECM formation, composition, or degradation were up-regulated more than twofold in the lymphatic vessels in comparison to the blood vessels (Tables S2 and S3). Preferential expression of Efemp1, Spock3, and Nid2 in lymphatic in comparison to blood vessels was further confirmed by immunofluorescence of mouse skin or Western blot analysis of primary ECs (Fig. S1, A–D). Among the identified genes, we focused on Reelin that was found as being expressed almost fivefold higher in the lymphatic vessels compared with the veins (Table S2). Previously, specific Reelin immunoreactivity was reported in the developing lymphatic vessels in rat and human (Samama and Boehm, 2005). We further confirmed lymphatic specific expression of Reelin in vivo in murine embryonic (Fig. 2, A and A′) and postnatal (Fig. 2, B–E′; and Fig. S1, E–F′) lymphatic vasculature of the skin and mesentery. The apparent expression in arteries that was detected in microarray profiling (Table S2) was likely caused by contaminating nerve tissue expressing Reelin (Fig. S1, E–E‴).

Differential localization of Reelin in mature lymphatic capillaries and collecting vessels

Immunofluorescence for Reelin in the postnatal mesenteric and dermal lymphatic vasculature revealed intense perinuclear and

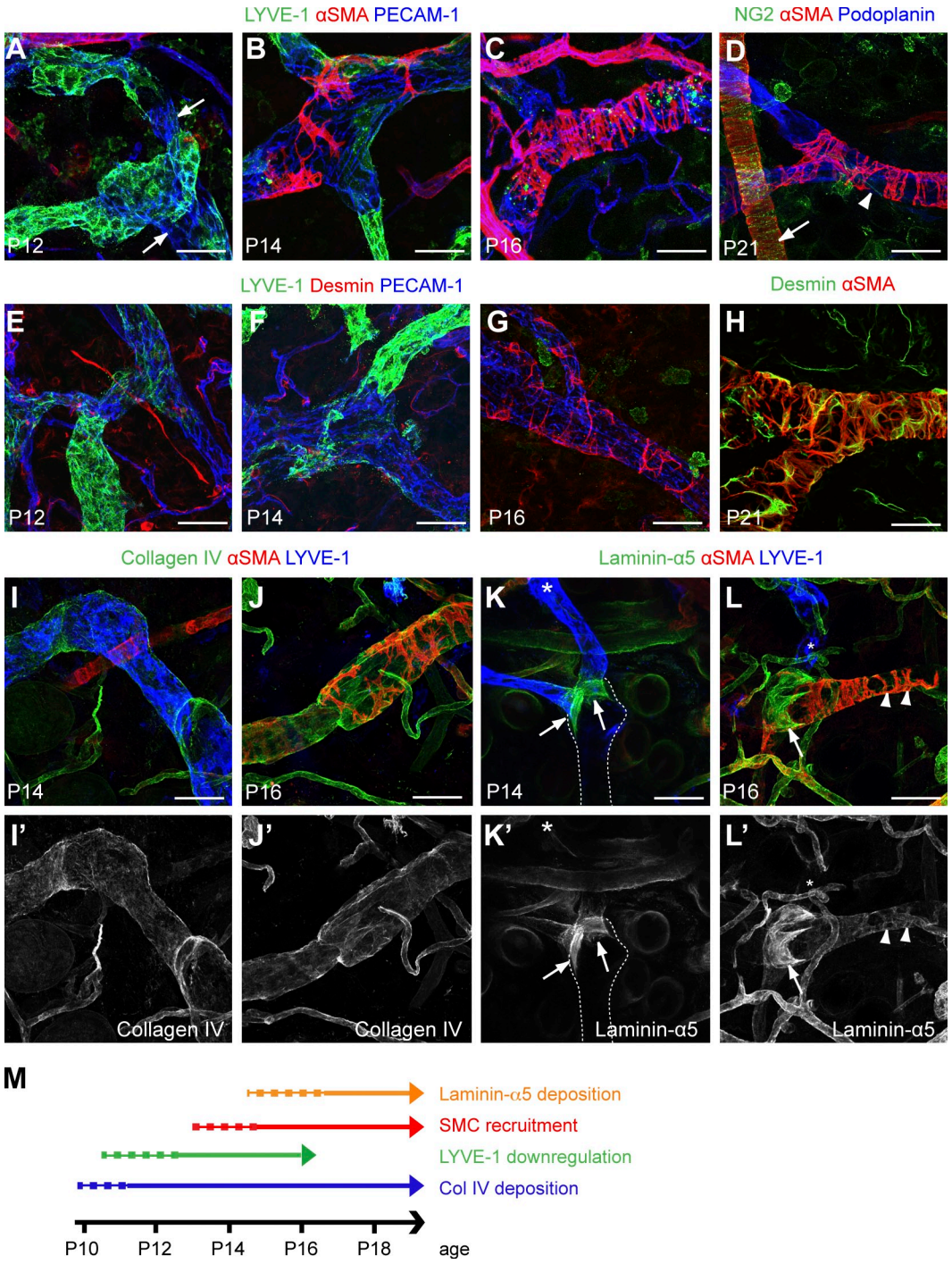

Figure 1. **SMC recruitment and ECM deposition during collecting vessel formation.** (A–H) Immunofluorescence staining of wild-type ear skin at the indicated stages (P12, P14, P16, or P21) with antibodies against LYVE-1 (green, A–C and E–G), α-SMA (red, A–D and H), desmin (red, E–G; green, H), PECAM-1 (blue, A–C and E–G), and Podoplanin (blue, D). Arrows in A indicate areas of LYVE-1 down-regulation before SMC recruitment. The arrow in D indicates an NG2-positive blood vessel, and the arrowhead in D indicates an NG2-negative collecting vessel. P, postnatal day. (I–L) Immunofluorescence staining of wild-type ear skin at P14 (I, I′, K, and K′) and P16 (J, J′, L, and L′) with antibodies against Collagen IV (green I–J′), Laminin-α5 (green K–L′), α-SMA (red), and LYVE-1 (blue). Arrows show Laminin-α5 expression in luminal valves and arrowheads indicate expression of Laminin-α5 by SMC. The broken line in K outlines the LYVE-1$^-$ collecting vessel. The asterisks in K and L show LYVE-1$^+$ lymphatic capillaries. Bars, 50 µm. (M) Schematic timeline of dermal collecting lymphatic vessel differentiation.

punctuated staining in the blind-ended lymphatic capillaries (Fig. 2, B, B′, D, and D′). In contrast, the collecting vessels showed a weaker, diffuse Reelin immunoreactivity (Fig. 2, C, C′, E, and E′). To test if the differential protein distribution was related to different subcellular localization of Reelin, we used nonpermeabilized tissue, together with tyramide signal amplification (TSA) procedure, to allow specific staining of extracellular proteins. Under these conditions, low Reelin immunoreactivity was detected in the lymphatic capillaries (Fig. 2, F and F′), whereas intense, patchy labeling of collecting lymphatic

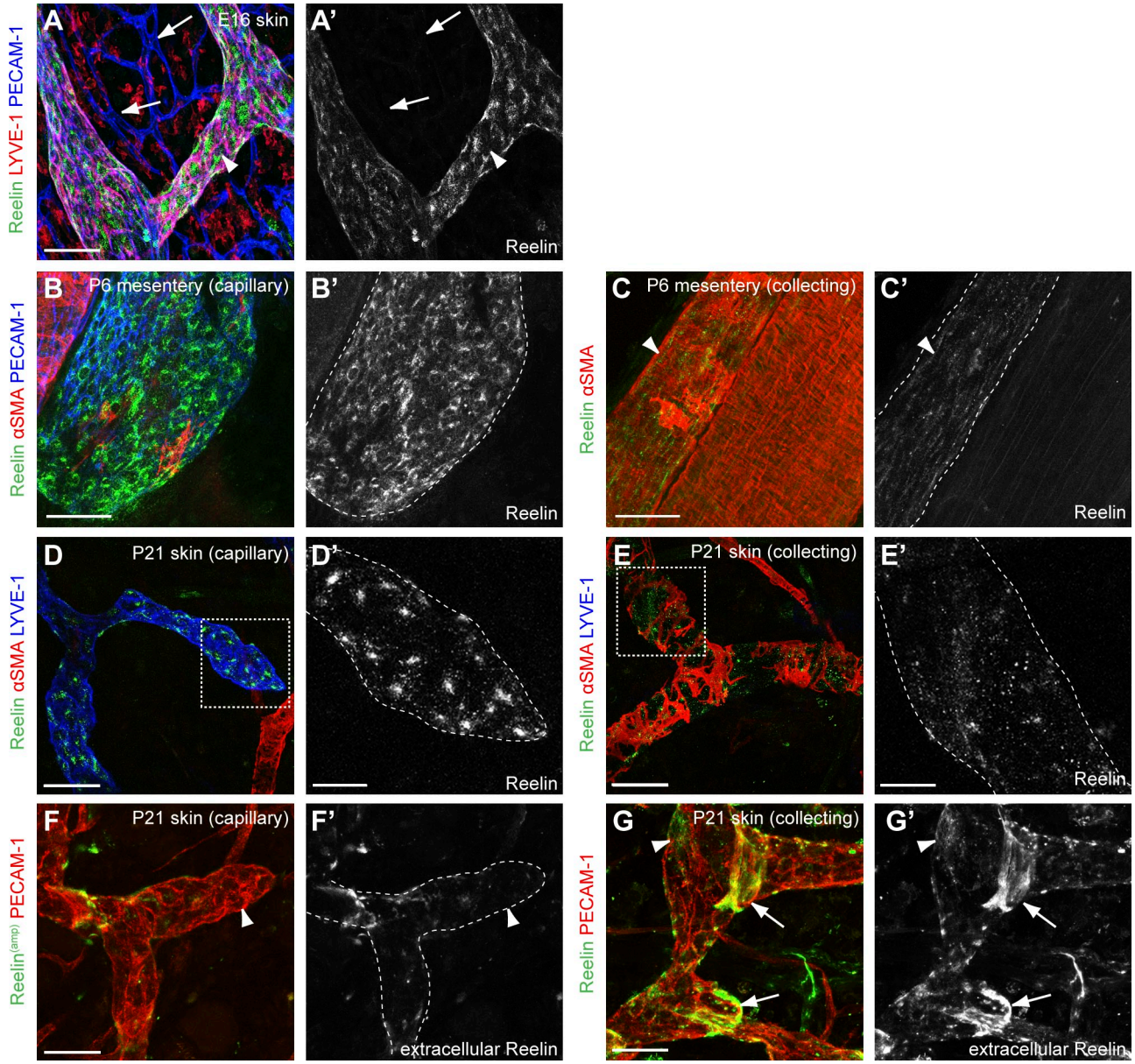

Figure 2. **Reelin is a lymphatic endothelial-specific matrix molecule that shows differential distribution in lymphatic capillaries and collecting vessels.** (A and A′) Immunofluorescence of E16 dorsal skin for Reelin (green), LYVE-1 (red), and PECAM-1 (blue). Arrowheads and arrows indicates Reelin-positive and -negative lymphatic and blood vessels, respectively. (B–G′) Immunofluorescence staining of P6 mesentery (B–C′) and P21 ear-skin (D–G′), with antibodies against Reelin (green) and α-SMA (red). Blue staining (in B) is for PECAM-1 and (in D–E′) for LYVE-1. Boxed areas in D and E are magnified in D′ and E′, showing Reelin expression only. Vessel borders are highlighted by broken lines in B′, C′, D′, E′, and F′). Tissue was unpermeabilized in F–G′ to detect extracellular proteins, and the fluorescent signal was amplified using TSA technology. The arrowhead in F indicates weak Reelin immunoreactivity outside capillary LECs. Bars: (A, D, E, F and G) 50 µm; (B and C) 500 µm; (D′ and E′) 20 µm.

vessels was observed (Fig. 2, G and G′). Particularly strong immunoreactivity for extracellular Reelin (Fig. 2, G and G′), but not for total Reelin protein (Fig. S1, E and E′), was observed around lymphatic valves, which suggests that Reelin is preferentially deposited in the valve regions, possibly by binding to specific matrix components that are enriched in these areas. Co-staining with cell compartment–specific markers suggested that intracellular Reelin in lymphatic capillaries resided predominantly in the endoplasmic reticulum (Fig. S1, G and H), similar to what has been reported in neurons (Tinnes et al., 2011). Together, these data suggest that Reelin is secreted by the lymphatic ECs (LECs) into the ECM of the collecting vessels, but remains intracellular in the endothelia of lymphatic capillaries.

SMC contact activates Reelin signaling by stimulating its secretion from lymphatic endothelia and proteolytic processing

We conjectured that the secretion of Reelin into the ECM could be related to SMC recruitment in the collecting vessels. To test this, we analyzed Reelin expression and secretion by the LECs that were either cultured alone or together with SMCs.

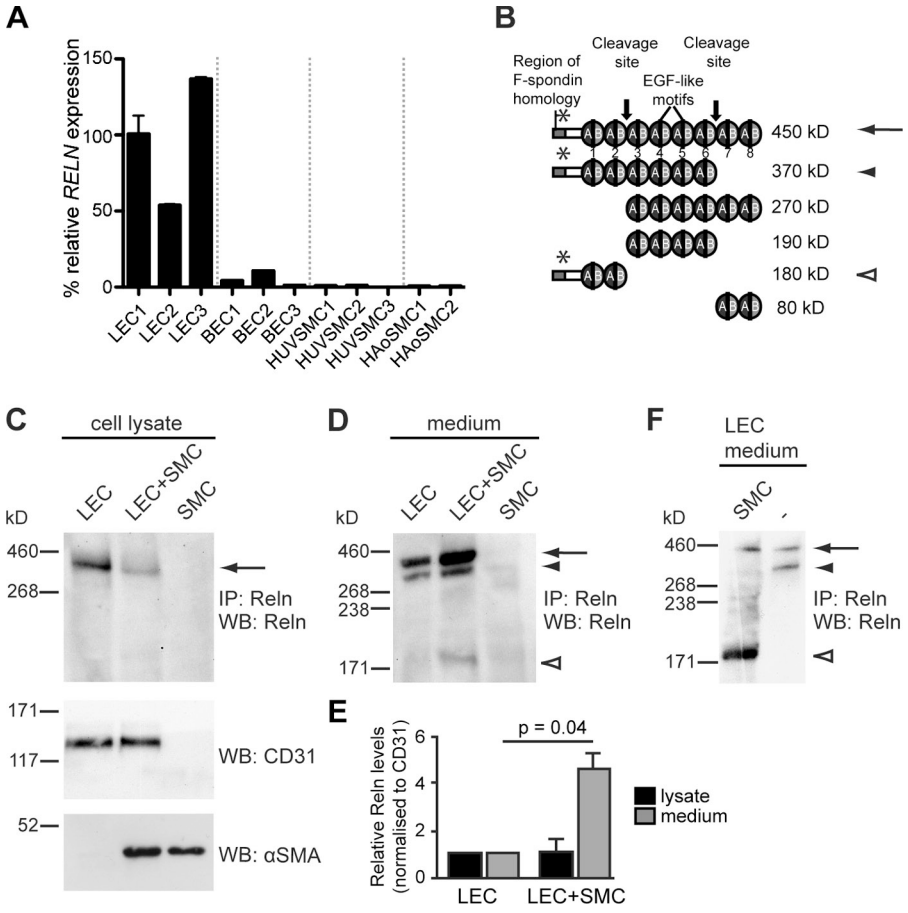

Figure 3. **Reelin secretion and processing is stimulated by SMC contact.** (A) qPCR analysis showing relative *RELN* expression in three independent samples of LEC, BEC, and HUVSMC and two samples of HAoSMC. Mean ± SEM is plotted (error bars). (B) Schematic of Reelin structure, showing antibody binding sites (asterisks), cleavage sites, and products. The arrows and arrowheads indicate polypeptides that are visualized in Western blotting: arrow, full-length protein; arrowhead, C-terminally cleaved polypeptide; open arrowhead, N- and C-terminally cleaved polypeptide. Adapted from Jossin et al. (2007). (C and D) Analysis of whole-cell lysate (C) and medium (D) of LEC and SMC cultured either alone or together by immunoprecipitation and Western blotting with antibodies to Reelin. The arrows indicates full-length Reelin, arrowheads indicate cleavage products. Analysis of whole cell lysate in C by Western blotting with antibodies to CD31/PECAM-1 (for LEC) and α-SMA (for SMC) show that equivalent numbers of cells were used. (E) Quantification of Reelin protein levels, normalized to CD31/PECAM-1, in whole cell lysate (black bars) and culture medium (gray bars). Data represent mean (n = 3) ± SEM (error bars). (F) Analysis of LEC-conditioned medium alone or after incubation with SMC. Note the cleavage product of 180 kD only in the presence of SMC (open arrowhead).

Lymphatic endothelial-specific expression of Reelin was maintained in vitro, as assessed by quantitative PCR (qPCR) analyses of RNA extracted from primary human LECs, blood vascular ECs (BECs), and SMCs (Fig. 3 A). In addition, immunoprecipitation and Western blot analysis using an antibody that recognizes an epitope at the N terminus of Reelin (Fig. 3 B) confirmed that only LECs produced Reelin protein (Fig. 3 C). Analysis of the medium from LECs revealed secretion of full-length 450-kD Reelin polypeptide that was partially processed by cleavage within the C terminus (Fig. 3 B; Jossin et al., 2007) to give rise to a smaller fragment of 370 kD (Fig. 3 D). When LECs were co-cultured with SMCs, secretion of full-length Reelin into the medium was increased, with a corresponding increase in the production of the 370-kD fragment, whereas the production of Reelin was not affected (Fig. 3, D and E). In addition, a second processing event in the N terminus resulted in the formation of a 180-kD fragment (Fig. 3, B and 3D) and a central Reelin fragment, which is capable of binding and activation of the canonical Reelin receptors ApoER2 and VLDLR (Jossin et al., 2007). Incubation of supernatant from LECs with SMCs confirmed that SMCs can mediate the second N-terminal processing event (Fig. 3 F). No increase in Reelin secretion or processing was observed when LECs were cultured in the conditioned medium collected from the SMCs, or on extracellular matrices produced by fibroblasts (unpublished data), which suggests that the effect was not mediated by an SMC-derived secreted protein. Together, these results demonstrate that SMC contact stimulates the secretion of Reelin from the LECs and its proteolytic processing, which suggests that SMC recruitment to the collecting lymphatic vessels activates Reelin signaling.

Defective collecting lymphatic vessel formation in Reelin-deficient mice

To investigate the physiological function of Reelin in lymphatic vasculature, we analyzed the dermal lymphatic vessels in Reelin (encoded by *Reln*)-deficient *Reeler* mice (D'Arcangelo et al., 1995). The mature dermal lymphatic vasculature is composed of three types of vessels: collecting vessels, precollectors, and capillaries. Precollectors share features of both capillaries and collecting vessels; in most cases they are LYVE-1–positive vessels that contain luminal valves but no SMCs. They often abruptly branch off the main LYVE-1–negative collecting vessel (Fig. 4 A, see also Fig. 4 F). However, in some cases, transition from one type of vessel to another is more gradual; individual α-SMA–positive cells can be found attached on vessels that contain some LYVE-1$^+$ ECs (unpublished data). Notably, however, SMCs are rarely found directly attached to LYVE-1$^+$ LECs, or on uniformly LYVE-1$^+$ vessels. Because the definition of precollecting vessel is ambiguous, in this study we considered only two vessel categories that we defined as collecting vessels based on the presence of α-SMA$^+$ SMCs and as capillaries based on positive LYVE-1 immunoreactivity.

We observed an apparently normal LYVE-1–positive dermal lymphatic capillary network in the ears of the *Reln*-deficient

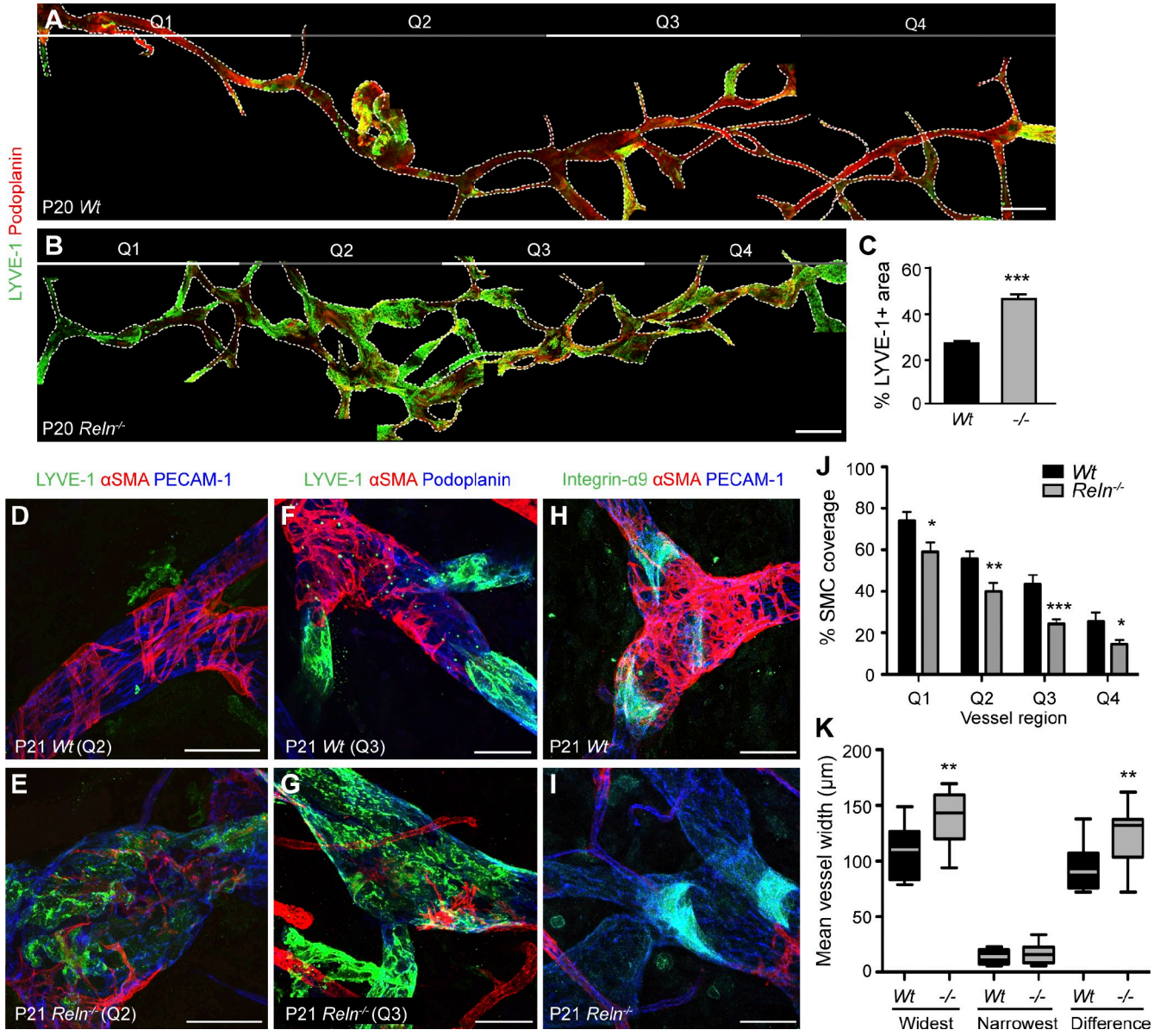

Figure 4. **Reduced SMC coverage and defective collecting lymphatic vessel differentiation in *Reln*-deficient mice.** (A, B, and D–I) Immunofluorescence of ear skin from wild-type (A, D, F, and H) and *Reln*$^{-/-}$ (B, E, G, and I) mice for the indicated proteins. For A and B, individual images (projections of confocal z stacks) were aligned to trace the entire collecting vessel from the proximal (Q1) to distal (Q4) end, and the overlapping blood vasculature was blacked out for clarity (original images are shown in Fig. S2). Broken lines outline the collecting vessels. (C) LYVE-1 immunoreactivity in wild-type and *Reln*$^{-/-}$ vessels (mean ± SEM [error bars]; $n = 6$ vessels). (J) SMC coverage in vessel quarters (mean ± SEM; $n \geq 12$ vessels). (K) Quantification of widest and narrowest vessel points and the difference between the two ($n \geq 12$ vessels). The boxes represent interquartile range, lines indicate mean, and whiskers indicate minimum and maximum values. *, $P < 0.05$; **, $P < 0.01$; ***, $P < 0.005$. Bars: (A and B) 200 µm; (D–I) 50 µm.

mice (Fig. S2, A and B). To allow unambiguous distinction of collecting vessels, we traced the entire vessel from the proximal to the distal end of the ear. In comparison to LYVE-1–negative collecting vessels in wild-type mice, *Reln* mutant vessels maintained an abnormally high level of LYVE-1 (Fig. 4, A–C; and Fig. S2, E and F). In addition, *Reln* mutants showed reduced SMC coverage when compared with wild-type vessels (Fig. 4, D–G and J). Although a similar proximal-to-distal decrease was observed, in each vessel quarter the SMC coverage was significantly lower in *Reln* mutant compared with the wild type (Fig. 4 J). The early differentiation of dermal collecting vessels appeared normal in *Reln* mutants, as indicated by deposition of Collagen IV and formation of luminal valves (Fig. S2, G–H′; and Fig. 4, H and I); however, deposition of SMC-derived Laminin-α5 was strongly decreased (Fig. S2, I–J′). In addition, *Reln* mutants displayed irregular lymphatic vessel diameter, with abnormal constrictions and swellings (Fig. 4, B and K). These defects were not secondary to nervous system defects because normal patterning of the nerves was found in *Reln* mutant ears (Fig. S2, C and D). In contrast to the dermal collecting lymphatic vessels, the large collecting vessels of the mesentery appeared normal in *Reln*-deficient mice, as indicated by normal morphology and SMC coverage (Fig. S3). In summary, these data show that *Reln* deficiency leads to specific defects in dermal collecting lymphatic vessel formation.

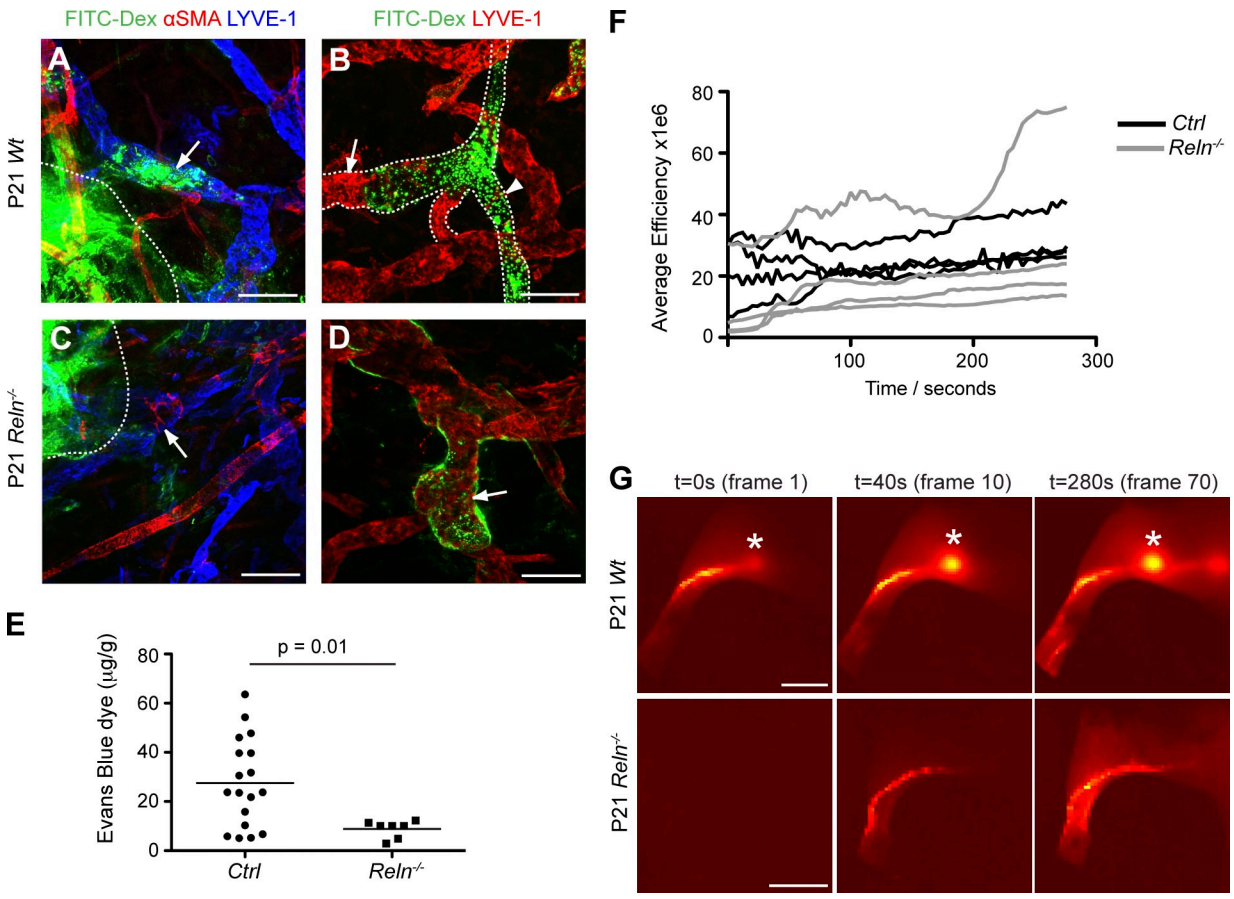

Figure 5. **Functional impairment in *Reln*$^{-/-}$ collecting lymphatic vessels.** (A–D) P21 wild-type (A and B) and *Reln*$^{-/-}$ (C and D) ear skin, injected with FITC-dextran (green) and costained with antibodies against α-SMA (red; A and C) and LYVE-1 (blue, A and C; and red, B and D). The broken line in A and C indicates the injection site, and arrows point to adjacent lymphatic vessels. Arrows in B and D point to LYVE-1–positive capillaries, and the arrowhead in B indicates an LYVE-1–negative collecting vessel filled with FITC-dextran. The broken line in B outlines the collecting vessel and its connection to LYVE-1^{+} capillaries (not outlined). (E) Quantification of Evans blue dye content in inguinal lymph nodes of control and *Reln*$^{-/-}$ mice after 5 min of injection into the hind limb footpad. Values from individual lymph nodes and mean values are plotted (error bars; *n* = 11 [*Ctrl*] and 6 [*Reln*$^{-/-}$] mice). (F) Efficiency of fluorescent signal, representing efficiency of lymphatic flow, in a defined region of a vessel after ICG injection into the hind limb footpad over time. (G) Representative images of control and *Reln*$^{-/-}$ hind limbs after ICG dye injections at three time points (excluding a 6–8-s delay before recording was started). In control but not in *Reln*$^{-/-}$ mice, the dye reached the inguinal lymph node (asterisks). Bars: (A–D) 100 µm; (G) 0.5 cm.

Impaired lymphatic vessel function in Reelin mutant mice

To assess if the observed morphological defects affect lymphatic function in *Reln* mutants, we investigated the uptake and transport of large-molecular-weight fluorescent dextran–injected intradermally in the ear. In wild-type mice, the dye was quickly taken up into the vessels surrounding the injection site (Fig. 5 A). However, except for in the immediate vicinity of the injection site, dye was rarely seen in LYVE-1–positive capillaries, whereas the collecting vessels were strongly positive (Fig. 5 B). In contrast, in *Reln*$^{-/-}$ mice we frequently observed no dye in vessels near the injection site (Fig. 5 C), which suggests impaired lymphatic function. When dye was taken up, it was retained in LYVE-1–positive vessels (Fig. 5 D). We also observed dye at the vessel edges in the mutant ear (Fig. 5 D), which may be indicative of dye leakage from the vessel and retention within the BM, further suggesting functional deficiency in the collecting vessels of these mice. It is possible that discontinuous coverage of SMC around collecting lymphatic vessels may aid solute exchange and therefore increase collecting vessel "leakiness" (Scallan and Huxley, 2010). To further assess the potential impairment of lymphatic function, we used the Evans blue method to allow quantitative measurement of dye content of the inguinal lymph nodes after hind limb footpad injection. Control mice showed significantly more dye in the lymph nodes when compared with the *Reln*$^{-/-}$ mice (Fig. 5 E). In addition, we performed real-time imaging of the uptake of indocyanine green (ICG) dye by lymphatic vessels by measuring the increase in the fluorescent signal in the vessel over time after injection of the dye into the hind limb footpad. Abnormal dye uptake was observed in the *Reln* mutant mice compared with their control littermates (Fig. 5 F). All except one *Reln*-deficient mouse displayed reduction in the rate of lymphatic flow, whereas one showed an abnormally fast dye uptake. In control littermates, the dye reached the inguinal lymph nodes within seconds (Fig. 5 G and Fig. S4 A). In contrast, in most *Reln* mutants, no ICG dye was detectable in the lymph nodes at the end of 5 min of imaging (Fig. 5 G and Fig. S4 B). In spite of impaired lymphatic function, no apparent edema or ascites formation could be observed in the mutant mice (unpublished data).

Reelin induces production of SMC recruitment factor MCP-1 in LECs via a noncanonical signaling pathway

In the nervous system, Reelin mediates its functions via two members of the low-density lipoprotein receptor family, VLDLR and ApoER2 (Trommsdorff et al., 1999). Both receptors were expressed in cultured primary SMCs and LECs (Fig. S5 A). In addition, VLDLR was expressed in lymphatic endothelia in vivo (Fig. S5, B–C′). This suggests that either cell type—LEC or SMC—could therefore respond to Reelin to regulate SMC recruitment during collecting vessel formation. However, although LEC-conditioned medium promoted SMC migration in a transwell assay, this was not affected by a function-blocking antibody to Reelin (Fig. 5 E and S5 D). Furthermore, Reelin did not stimulate migration of SMCs (Fig. S5 D), which suggests that Reelin is not the LEC-derived factor responsible for SMC recruitment. We therefore tested a possibility that Reelin acts in an autocrine fashion in LECs to induce production of SMC recruitment factors. Indeed, we found a transient increase in the expression of *MCP1/CCR2*, a known regulator of SMC recruitment and migration (Fig. S5 D; Religa et al., 2005; Ma et al., 2008; Aplin et al., 2010), in LECs upon Reelin stimulation (Fig. 6, A and B), whereas the expression of four other genes implicated in SMC recruitment was not affected (Fig. 6, A and B). Increased Angiopoietin-2 expression that was induced similarly by control and full-length Reelin containing 293 supernatant was likely caused by a high level of VEGF produced by these cells (Kärpänen et al., 2006), which has previously been shown to stimulate Ang-2 expression in LECs (Veikkola et al., 2003). Notably, *MCP1* expression showed only a modest increase upon stimulation with the central Reelin fragment (Fig. 6 A), which suggests that the canonical Reelin signaling pathway was not responsible for this effect. In agreement, analysis of *Vldlr* and *Apoer2* double mutant mice revealed normal lymphatic vasculature (Figs. 5 G; Fig. 6, C and D; and Fig. S5 F). In addition, mouse mutants lacking Dab1, an intracellular adaptor molecule activated in response to Reelin signaling, showed normal lymphatic vessels (Fig. 6 E and Fig. S5 H). All parameters measured were normal (Fig. 6, F–H), with the exception that the $Vldlr^{-/-}$;$Apoer2^{-/-}$ vessels showed a modest decrease in SMC coverage in the distalmost quarter (Fig. 6 F). In addition, lymphatic function was not impaired in these mice (Fig. S5 I). In summary, these results suggest that Reelin acts in an autocrine fashion in the LECs to regulate SMC recruitment and collecting vessel differentiation (Fig. 7). Interestingly, unlike in the nervous system, the canonical signaling pathway is not required for Reelin signaling in lymphatic vessels, which suggests the involvement of alternative receptors.

Discussion

Although proteins of the vascular BM are known to play diverse and essential roles in the maintenance of both the structural and biological function of the vessel, the composition and function of the lymphatic BM remains poorly characterized. Furthermore, differences in the BM surrounding different types of lymphatic vessels have been largely ignored, yet they are likely important because of the distinct functions of lymphatic capillaries and collecting vessels in mediating fluid absorbance and transport, respectively (Jurisic and Detmar, 2009; Tammela and Alitalo, 2010). In this study, we identify Reelin as the first lymphatic specific ECM protein and demonstrate its important function in the formation of functional collecting vessels.

Reelin is a large glycoprotein previously implicated in the development of the nervous system. Our analyses revealed that Reelin is additionally widely expressed in the lymphatic vasculature, both during development and in adult tissues. Although Reelin was produced by LEC in both the capillaries and collecting vessels, only the latter showed efficient secretion. Consistent with this, *Reln*-deficient mice had normal lymphatic capillaries but exhibited specific dermal collecting vessel defects, characterized by reduced SMC coverage and high expression of lymphatic capillary marker LYVE-1. Interestingly, SMCs were frequently found in direct contact with LYVE-1^+ LECs in the mutant but not in wild-type vessels. Notably, however, the largest collecting vessels, such as mesenteric lymphatic vessels that acquire more elaborate and continuous smooth muscle coverage, were apparently normal in *Reln* mutants, which suggests that there are different requirements for the formation of vessels of different calibers. We also noted a difference in the initiation of collecting vessel maturation in these two tissues. Although the developing dermal collecting vessels underwent a gradual increase in SMC coverage and concomitant decrease in LYVE-1 expression in a proximal-to-distal direction over a period of several days, the mesenteric lymphatic vessels rapidly acquired SMCs along their entire length, which was only later followed by down-regulation of LYVE-1 expression. These observations further suggest that the mechanisms regulating collecting vessel formation may differ depending on the caliber of the vessel and tissue environment.

Previous data on various mouse models lacking key components required for mural cell (MC) recruitment attest to their importance in the formation and maintenance of functional blood vessels (Hellström et al., 2001). However, because of embryonic lethality, none of the MC-deficient mice described so far have allowed the investigation of the importance of lymphatic SMC in vivo. Our study describes for the first time a mouse model that shows a lymphatic-specific deficiency in SMCs, which occur in the absence of blood vascular or other major lymphatic defects. Concurrent with reduced SMC coverage, the *Reln*-deficient collecting vessels were enlarged and displayed irregular vessel diameters. Such defects are consistent with phenotypes described for pericyte-deficient blood vessels (Hellström et al., 2001), which suggests that lymphatic SMC may have similar roles in the maintenance of vessel stability to those of the blood vascular system. However, important functional differences between lymphatic and blood vascular SMC exist. Although blood flow is generated by the beating heart and the vascular SMCs are involved in regulating vascular tone, the lymphatic vessels themselves must generate the force required for lymph propulsion (for review see von der Weid and Zawieja, 2004). This action is dependent on lymphatic SMCs, which, unlike the vascular SMCs, are able to undergo

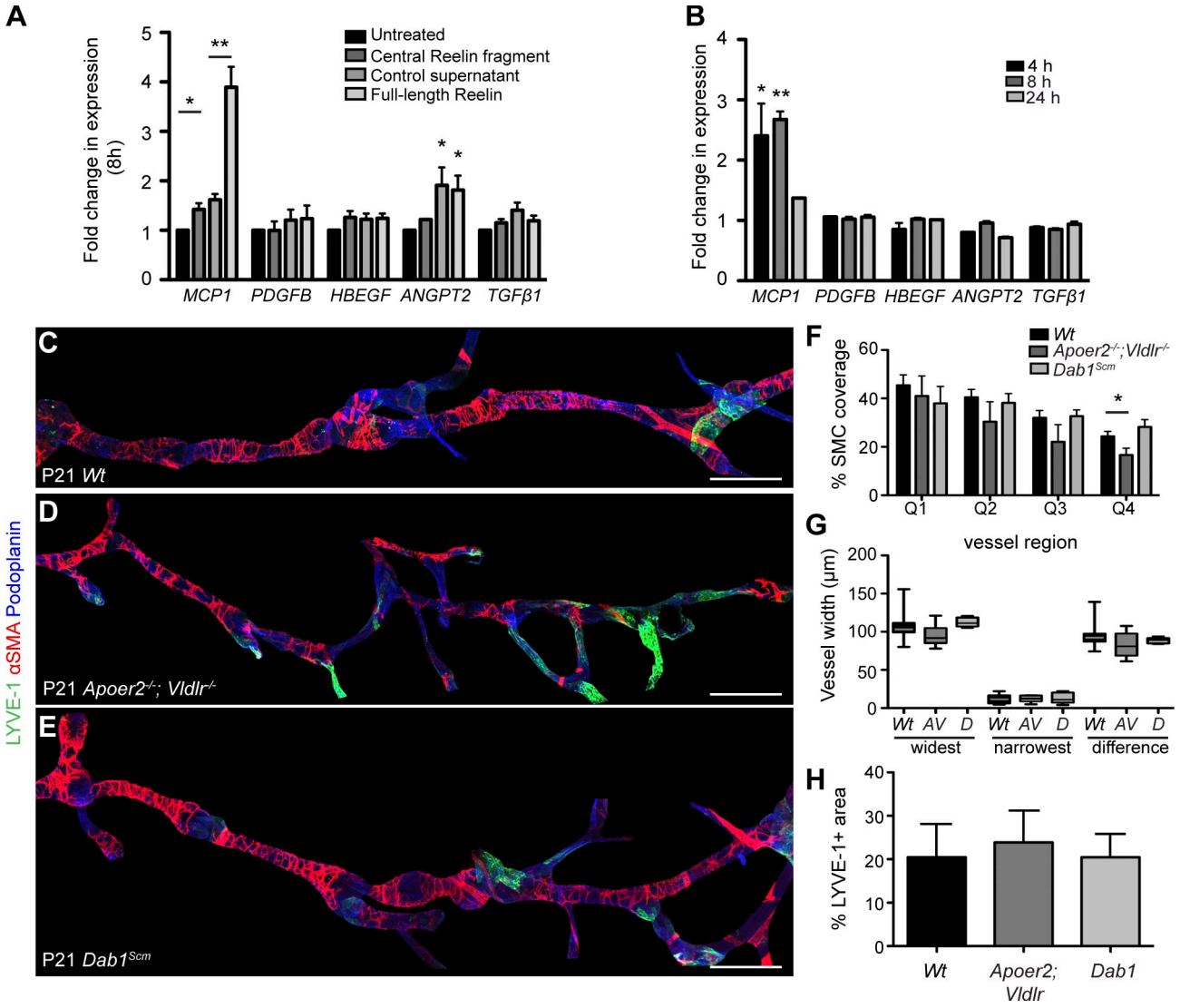

Figure 6. **LECs respond to Reelin via noncanonical signaling pathway.** (A and B) Fold change in expression of SMC recruitment genes after Reelin stimulation. Note the strong increase in *MCP1* expression at 4 and 8 h in cells stimulated with full-length Reelin containing supernatant from HEK 293 cells only. The mean ± SEM of three experiments is plotted (error bars). *, $P < 0.05$; **, $P < 0.001$. (C–E) Immunofluorescence staining of P21 ear skin from wild-type (C), *Apoer2*$^{-/-}$*;Vldlr*$^{-/-}$ (D), and *Dab1*^{Scm} (E) mice using LYVE-1 (green), α-SMA (red), and Podoplanin (blue) antibodies. Individual images were aligned to trace the vessel from the proximal to the distal end, and overlapping blood vasculature was blacked out for clarity. A segment from the middle section of each vessel is displayed (original images are shown in Fig. S5). (F) SMC coverage in vessel quarters (mean ± SEM [error bars]; $n \geq 6$ vessels per genotype). *, $P = 0.04$. (G) Quantification of the widest and narrowest vessel points and the difference between the two. Boxes represents interquartile range, lines indicates mean, and whiskers indicate minimum and maximum values. (H) LYVE-1 immunoreactivity in collecting vessels (mean ± SEM [error bars]; $n \geq 6$ vessels). All differences in F–H were nonsignificant, except where indicated. Bars, 200 μm.

both tonic and phasic contractions (Wang et al., 2009). The impaired lymphatic function may imply that, in addition to the observed morphological abnormalities, *Reln* deficiency can directly affect SMC contractility and lymph pumping. These findings may have clinical significance, as congenital lymphedema has been observed in some human patients carrying mutations in the *RELN* gene (Hong et al., 2000).

In spite of intense studies during the past decade, the exact cellular function of Reelin has remained unclear. In early corticogenesis, Reelin stimulates neuronal migration by attracting leading processes and inducing their branching and attachment to the ECM (Ogawa et al., 1995; Tissir and Goffinet, 2003; Franco et al., 2011). In contrast, at later stages, when the migrating neurons reach their destination at the marginal zone of the cortex, Reelin acts as a stop signal by inducing neuronal detachment from radial glial scaffold and stabilization of the cytoskeleton (Hartfuss et al., 2003; Chai et al., 2009; Zhao and Frotscher, 2010). These opposite functions of Reelin may be explained, at least in part, by binding and activation of different receptors: VLDLR and ApoER2 (Hack et al., 2007). Proteolytic processing by matrix metalloproteinases may also play an important role in regulating diffusion and receptor-binding properties of Reelin (Lambert de Rouvroit et al., 1999; Jossin et al., 2007; Tinnes et al., 2011). Although the central part of Reelin binds VLDLR and ApoER2, the N-terminal region mediates protein aggregation and has been suggested to regulate signaling by anchoring the protein to the

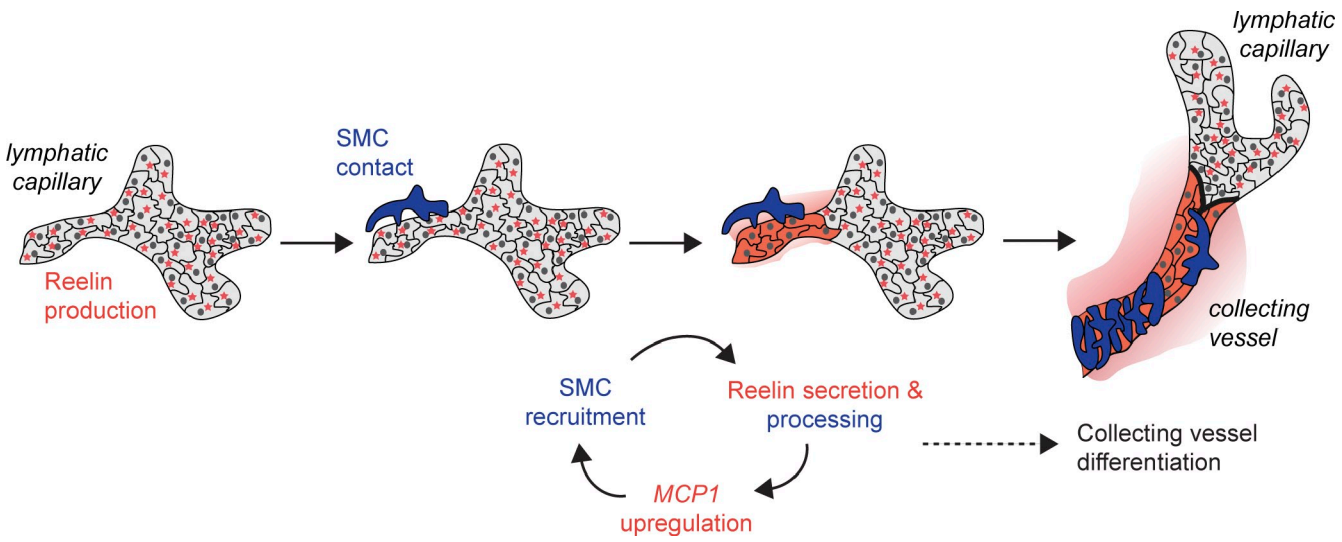

Figure 7. **Model of Reelin signaling during collecting lymphatic vessel formation.** Reelin (red stars) is produced by LEC (gray cells). Upon SMC (blue cell) contact, Reelin is secreted from LEC (red cells) and cleaved to release diffusible fragments (red gradient). Reelin can stimulate expression of *MCP1* in LECs to enhance further SMC recruitment.

ECM (Utsunomiya-Tate et al., 2000; Kubo et al., 2002; Zhao and Frotscher, 2010). Because the cleavage products generated in LEC/SMC cultures were identical to those documented in the nervous system (Jossin et al., 2007), the same mechanism of processing is likely. However, although functionally important (Jossin et al., 2007), it is unclear how the processing is regulated in vivo and whether the individual cleavage products have specific, or even opposite functions. Interestingly, mechanisms where proteolytic processing produces protein fragments that exhibit opposing effects on angiogenesis to those of the parental molecule have been described for a subclass of vascular ECM proteins (for review see Kalluri, 2003).

In the developing nervous system, Reelin is produced mainly by Cajal-Retzius neurons in the cortex, where it instructs newly born neurons to assume their position and orientation (D'Arcangelo et al., 1995; Tissir and Goffinet, 2003). During this process, the neurons are intimately apposed to radial glial cells that form a scaffold along which the neuroblasts migrate, and both cell types rely on Reelin signaling to direct correct patterning of the cortex (Hartfuss et al., 2003; Tissir and Goffinet, 2003; Keilani and Sugaya, 2008; Zhao and Frotscher, 2010). In the lymphatic system, we found that Reelin was produced exclusively by ECs, while its release and proteolytic processing was stimulated by the adjacent SMCs. This suggests a mechanism by which Reelin signaling is activated via communication of the two cell types that form the collecting vessels. We further found that LECs, in turn, respond to Reelin by upregulating the expression of monocyte chemotactic protein 1 (MCP1), a factor known to promote SMC migration and proliferation (Religa et al., 2005; Ma et al., 2008; Aplin et al., 2010). This suggests an autocrine function of Reelin in the LECs in controlling the expression of factors involved in SMC recruitment. Interestingly, although the canonical Reelin receptors VLDLR and ApoER2 were expressed in the lymphatic vasculature, *Apoer2;Vldlr* double mutant mice did not recapitulate the phenotype observed in *Reln*-deficient lymphatic vessels. Normal lymphatic development in *Apoer2;Vldlr* double mutant mice, which display an identical neurological phenotype compared with *Reln* mutants (Trommsdorff et al., 1999), further indicates that the collecting vessel defects in *Reln*-deficient mice are not secondary to nervous system defects or the failure of these mice to gain weight, but instead suggests involvement of alternative Reelin receptors.

In summary, we have demonstrated an unexpected function of Reelin in regulating the formation of functional larger-caliber lymphatic vessels. Our results have uncovered a mechanism by which a specific signaling pathway is activated by communication between the two cell types of lymphatic vessels—EC and SMC—and demonstrate for the first time that SMCs play an important role in regulating lymphatic morphogenesis and function.

Materials and methods

Antibodies

The antibodies used for immunofluorescence were rat antibodies to mouse platelet EC adhesion molecule 1 (PECAM-1; MEC3.1, BD); rabbit antibodies to mouse Laminin-α5 (provided by L. Sorokin, University of Münster, Münster, Germany; Ringelmann et al., 1999), Desmin (Abcam), Collagen IV (AbD Serotec), GFP (Invitrogen), LYVE-1 (ReliaTech), Erp57 (Abcam), and Golph4 (Abcam); rabbit antibody to human Efemp1 (Abcam); hamster antibodies to mouse PECAM-1 (Millipore) and Podoplanin (Developmental Studies Hybridoma Bank); goat antibodies to mouse Integrin-α9, Reelin, and VLDLR (all from R&D Systems); mouse antibody to mouse acetylated α-tubulin (Abcam; used in conjunction with mouse-on-mouse blocking reagents [Vector Laboratories]); and Cy3-conjugated mouse antibody against α-SMA (Sigma-Aldrich). Secondary antibodies conjugated to Cy2, Cy3, or Cy5 were obtained from Jackson ImmunoResearch Laboratories, Inc. Antibodies used for Western blot analysis were rabbit antibodies to human Efemp1 (Abcam), Nidogen2 (Immundiagnostik), and Spock3 (Abcam), and mouse antibody to human α-tubulin (Sigma-Aldrich).

Mice

Reeler (*Reln*^{rl}) and *Dab1*^{scm} (*A/A-Dab1*^{scm}*/J*) mice were obtained from The Jackson Laboratory. *Apoer2*$^{-/-}$*;Vldlr*$^{-/-}$ mice were obtained by cross-breeding of mice lacking *Apoer2* or *Vldlr*, which carry an insertion of a Neomycin cassette to replace exons 17 and 18, or into exon 5, leading to deletion of part of the coding sequence and disruption of the reading

frame, respectively (Frykman et al., 1995; Trommsdorff et al., 1999). Both lines were provided by J. Herz (University of Texas Southwestern Medical Center, Austin, TX). *Vegfr3*^{lz} mice in which the first coding exon of *Vegfr3* gene was replaced by a lacZ cassette were provided by K. Alitalo (University of Helsinki, Helsinki, Finland). The mice were maintained on C57BL/6J background except for *Dab1*^{scm}, which were on C3HeB/FeJ* DC/Le background. All three mutant strains lacking components of the Reelin signaling pathway exhibited an ataxic gait and tremors starting around two weeks of age. In addition, homozygous *Reeler* and *Apoer2*$^{-/-}$*;Vldlr*$^{-/-}$ mutant mice, but not *Dab1*^{scm} mutants, were smaller in size, weighing ~50–60% of the weight of the littermate controls at three weeks of age when most analyses were done. All mouse experiments were approved by the UK Home Office.

Microarray analysis

To identify lymphatic-specific ECM molecules, mesenteric arteries, veins, and lymphatic vessels were dissected from P7 wild-type (C57BL/6J) pups. Samples from nine animals (in two litters) were pooled. Total RNA was extracted and RNase-treated using an RNeasy Micro kit (QIAGEN) as per the manufacturer's instructions. 100 ng of RNA from two independent samples of each vessel was amplified using WT-Ovation Pico RNA Amplification System (NuGEN) and used for expression profiling using the Mouse exon 1.0 ST Array (Affymetrix), according to the manufacturer's instructions. The array data were processed using robust multiarray analysis (Irizarry et al., 2003) to generate gene-level signal estimates for core level probe sets. The arrays were normalized using quantile normalization and antigenomic probes used to model the background. Quantification was run using apt-1.10.0 from Affymetrix. Before statistical analysis, all Affymetrix control probe sets were removed. Gene changes were selected using a linear model where the standard errors were corrected using empirical Bayes shrinkage (fdr < 0.05). To identify lymphatic-specific transcriptional changes, we applied a nestedF procedure across the three contrasts, selecting genes significant in only the lymphatic groups (fdr < 0.05). Analysis was performed in Bioconductor (Gentleman et al., 2004) using Limma. Genes that were expressed at least twofold higher in different vessel types were searched in Uniprot database to identify proteins involved in ECM function or structure.

Immunostaining and X-Gal staining

For whole-mount immunostaining, tissue was fixed in 4% paraformaldehyde, permeabilized in 0.3% Triton X-100 in PBS, and blocked in PBST plus 3% milk. Primary antibodies were incubated at 4°C overnight in blocking buffer. After washing in PBSTx, the samples were incubated with fluorescence-conjugated secondary antibodies in blocking PBSTx plus 1% milk before further washing and mounting in Mowiol. Reelin staining in Figs. S1 (E–F′) and Fig. 2 (F–G′), and VLDLR staining in Fig. S5 (B–C′) were amplified using the TSA Fluorescein Tyramide Reagent Pack (PerkinElmer). For VLDLR staining (Fig. S5, B–C′), goat anti–mouse VLDLR antibody (R&D Systems) was pre-absorbed with a *Vldlr*$^{-/-}$ ear in TNB buffer (0.1 M Tris-HCl, pH 7.5, 0.15 M NaCl, and 0.5% blocking buffer [supplied in kit]) overnight before resuming normal amplification and staining protocol with a wild-type or mutant ear, as detailed above. Immunostaining for Fig. 2 (F–G′) was performed in the absence of Triton X-100. Staining for β-galactosidase activity in the lymphatic vessels in *Vegfr3*^{lz} mice was done using the substrate X-Gal (5-bromo-4-chloro-3-indolyl-β-D-galactopyranoside), and the images were acquired with a stereomicroscope (MZ16F) equipped with camera (DFC420C) and Microsystems software (all from Leica).

Image acquisition and quantitative analyses

Confocal images for Figs. 2 (B and C), 3 (G and H), 6 (C–E), S3 (A–D), and S5 (F–H), were acquired at room temperature using a confocal microscope (LSM 710; Zeiss Imager.Z2 and Zen 2009 software; Carl Zeiss) with a Plan-Apochromat 20×/0.8 NA air objective lens (Fig. 6, C–E; and Fig. S5, F–H) or DIC Plan-Apochromat 40×/1.3 NA water immersion objective lens (Fig. 2, B and C; Fig. 3, G and H; and Fig. S3, A–D). All other confocal images were acquired using an LSM 510 microscope (Axioplan 2 and LSM 510 version 3.2 software; all from Carl Zeiss), with Plan-Apochromat 10×/0.45 NA (Fig. S2, A–D) or 20×/0.75 NA (Fig. 4, A and B; and Fig. S2, E and F) air objective lenses, or Korr C-Apochromat 63×/1.2 NA (Fig. S1, G and H) or 40×/1.2 NA (all other images) water immersion objective lenses. All confocal images, except Fig. S1 (G and H), represent maximum projection images of confocal z stacks. For visualization of collecting vessels from the proximal to distal end of the ear, images were captured along the length of three randomly chosen collecting lymphatic vessels from *Reln*$^{-/-}$ (n = 5) and wild-type (n = 4) mice. The same analysis was performed for *Apoer2*$^{-/-}$*;Vldlr*$^{-/-}$, *Dab1*^{Scm}, and their respective littermate controls (n = 3 per each genotype, two vessels per mouse). The images were aligned and processed using Photoshop CS4 or CS5 (Adobe). Thresholding and quantification of the whole-vessel images were performed using MetaMorph Imaging software (Molecular Devices). An inclusive threshold was applied to the α-SMA channel so that the background was captured by, while all SMC were excluded from, the threshold. The length of the vessel was measured and divided into quarters. A region was drawn around each vessel segment, excluding overlapping blood vessels. The SMC coverage was calculated and subtracted from 100%. A similar thresholding technique was used to quantify the percentage of LVYE-1 immunofluorescence. The line tool in MetaMorph was used to measure the width of the widest and narrowest vessel points.

Analysis of lymphatic vessel function

For qualitative analysis of lymphatic vessel function, FITC-dextran (8 mg/ml in PBS; Sigma-Aldrich) was injected intradermally into the ears of anaesthetized mice and analyzed by confocal microscopy. For quantitative analysis, 2 µl of ICG dye (1% in dH_2O; Sigma-Aldrich) was injected into the footpads of anaesthetized mice inside the IVIS Spectrum Whole Body Imaging System (Caliper Life Sciences). Image acquisition and analysis was performed with Living Image 3 software (Caliper Life Sciences) using the following parameters: field of view 6.6, binning 8, and F-stop 2. 70 images were taken with a 2-s exposure time and no delay between acquisitions, which resulted in an image every 3–4 s. The efficiency of the fluorescent signal was measured in a region of interest (ROI) created around a small area of the lymphatic vessel above the knee. The mean efficiency against time was plotted using Prism 5 software, using 4 s as an interval. For the quantitative Evans blue assay, 2 µl Evan's blue dye (2%; Sigma-Aldrich) was injected into the hind limb footpad. After 5 min, the mice were sacrificed and inguinal lymph nodes were dissected. Both inguinal lymph nodes were weighed together and a mean value was used to calculate dye content in each of them separately. Each lymph node was placed in 5 µl formamide at 60°C for 24 h, followed by an absorbance reading at 620 nm. Evans blue concentration was calculated using a standard curve and presented as dye content per gram of tissue.

Cell culture

Human LECs, isolated from primary dermal microvascular EC cultures (PromoCell; Mäkinen et al., 2001), human umbilical venous SMCs (HUVSMCs; TCS Cellworks), and aortic SMCs (PromoCell) were cultured in endothelial or SMC growth medium (Promocell). For co-culture experiments, LEC were plated on fibronectin-coated plates at 50% confluency in IgG-stripped EC growth medium 4 h before an equal number of HUVSMC were added to the culture. Medium was collected and the cells were lysed 2 d after plating. Supernatant from HEK 293 cells transfected with pCrL (full-length mouse Reelin cDNA; a gift from Tom Curran, Joseph Stokes Jr. Research Institute, The Children's Hospital of Philadelphia, Philadelphia, PA) and untransfected control cells was concentrated 25× using an Amicon ultra-15 centrifugal filter unit (Sigma-Aldrich) and used for stimulation of LEC or SMC at dilution 1:20.

Reelin stimulation

LEC were starved overnight in serum-free EC growth medium, then supplemented with 0.2% BSA, hEGF-5, and HC-500, followed by stimulation with full-length Reelin supernatant from HEK 293 cells (diluted 1:20), control supernatant (diluted 1:20), or recombinant central Reelin fragment (R&D Systems) for 4, 8, or 24 h. RNA was extracted using RNeasy Mini kit (QIAGEN) according to the manufacturer's instructions and used for qPCR analysis using the following Taqman probes (Applied Biosystems): *PDGFB*, Hs00966522_m1; *ANGPT2*, Hs01048042_m1; *TGFβ1*, Hs00998133_m1; *HBEGF*, Hs00181813_m1; and *CCL2/MCP-1*, Hs00234140_m1 and *GAPDH*; Hs99999905_m1.

Western blot analysis

Cell growth medium was collected and clarified by centrifugation, and the cells were lysed in Triton X-100 lysis buffer (50 mM Tris, pH 7.5, 120 mM NaCl, 10% glycerol, 1% Triton X-100) supplemented with Complete Protease inhibitors (Roche). Cell lysate and growth medium were subjected to immunoprecipitation and/or Western blot analysis using mouse antibodies against human Reelin (EMD) and PECAM-1 (Dako), or Cy3-conjugated mouse anti–α-SMA (Sigma-Aldrich). Quantification was performed using ImageJ, and the ratio of Reelin in the lysate and medium, normalized to CD31/PECAM-1, was calculated for LEC/SMC co-culture relative to LEC cultured alone.

qPCR

RNA from LEC, BECs, human aortic SMCs (HAoSMCs), and HUVSMC was reverse transcribed using Superscript II Reverse transcription (Invitrogen) and random hexamers (Promega). cDNA was amplified by real-time qPCR (ABI 7900HT) using Platinum SYBR Green qPCR super mix-UDG with ROX reagent (QIAGEN). Each primer was used at a concentration of 0.4 µM. Cycling conditions were as follows: step 1, 2 min at 50°C; step 2, 10 min at 95°C; step 3, 15 s at 95°C; and step 4, 1 min at 60°C. Steps 3 and 4 were repeated 40 times. Data from the reaction was collected and analyzed using the complementary computer software. Relative quantifications of gene expression were normalized to expression of *GAPDH*. The primers were: *RELN*, 5′-GTTTTGCAAATTGGGAGCAT-3′ and 5′-CCGTTGTTGACGCTGTATTG-3′; *GAPDH*, 5′-GAAGGTGAAGGTCGGAGTC-3′ and 5′-GACAAGCTTCCCGTTCTCAG-3′; *PECAM1*, 5′-GAGAGGACATTGTGCTGCAA-3′ and 5′-GGGTTTGCCCTCTTTTTCTC-3′; and *LYVE1*, 5′-GCTTTCCATCCAGGTGTCAT-3′ and 5′-AGCCTACAGGCCTCCTTAGC-3′.

Transwell migration assay

Migration assay was performed using 6.5-mm Transwell with 8 µm polycarbonate membrane inserts (Corning) in a 24-well plate. The lower face of the membrane was coated with 1 µg/ml fibronectin (Sigma-Aldrich) before use. Confluent HUVSMC were serum-deprived in SMC growth medium containing 0.2% BSA for 22 h. 1×10^5 cells were seeded in the upper chamber and allowed to migrate toward EC growth medium (control) or conditioned medium collected from LECs over a 48-h period, full-length Reelin supernatant from HEK 293 cells (diluted 1:20), control supernatant (diluted 1:20), 10 ng/ml MCP-1 (R&D Systems), or 3 ng/ml PDGF-BB (R&D Systems) over a 23-h period. Reelin function was inhibited using blocking antibody against Reelin (CR-50, 50 µg/ml; MBL). Cells on the upper face of the membrane were removed and migrated cells on the lower face were fixed and stained with 0.5% crystal violet solution in 25% methanol. Images of the filters were acquired with a stereomicroscope (MZ16 F) equipped with a camera (DFC420C) and Microsystems software (all from Leica). After photographing, the incorporated dye was solubilized in 0.2 ml sodium citrate solution, followed by absorbance reading at 550 nm.

Statistical analysis

P-values were calculated using unpaired two-tailed Student's *t* tests.

Online supplemental material

Fig. S1 shows the identification of extracellular matrix–associated proteins that are preferentially expressed in lymphatic vessels. Fig. S2 shows the characterization of *Reeler* phenotype in the skin. Fig. S3 shows the characterization of *Reeler* phenotype in the mesentery. Fig. S4 shows real-time imaging of lymphatic function in 3-wk-old control and *Reln*-deficient mice. Fig. S5 shows the involvement of Reelin signaling pathway components in lymphatic development and the effect of Reelin on SMC migration. Table S1 presents the validation of microarray data for known markers of lymphatic vessels, arteries, and veins. Table S2 shows genes associated with extracellular matrix that were differentially expressed in lymphatic and blood vessels. Table S3 shows the full dataset that was used for the validation of microarray hits. Online supplemental material is available at http://www.jcb.org/cgi/content/full/jcb.201110132/DC1.

We thank Joachim Herz for *Apoer2* and *Vldlr* mice, Michael Frotscher and Hans Bock for sending these mice to us, Kari Alitalo for *Vegfr3*^{lz} mice, Lydia Sorokin for Laminin-α5 antibodies, and Tom Curran for the pCrl plasmid. We thank the CRUK GeneChip Service Facility at Cancer Research UK Paterson Institute for performing the microarray experiments, Phil East for analysis of microarray data, Francois Lassailly for help with whole-body imaging, and the animal unit staff at the London Research Institute for animal husbandry.

This work was supported by Cancer Research UK (S. Lutter, S. Xie, F. Tatin, and T. Makinen) and EMBO Young Investigator Program (T. Makinen).

Submitted: 31 October 2011
Accepted: 2 May 2012

References

Aplin, A.C., E. Fogel, and R.F. Nicosia. 2010. MCP-1 promotes mural cell recruitment during angiogenesis in the aortic ring model. *Angiogenesis*. 13:219–226. http://dx.doi.org/10.1007/s10456-010-9179-8

Aszódi, A., K.R. Legate, I. Nakchbandi, and R. Fässler. 2006. What mouse mutants teach us about extracellular matrix function. *Annu. Rev. Cell Dev. Biol.* 22:591–621. http://dx.doi.org/10.1146/annurev.cellbio.22.010305.104258

Bazigou, E., S. Xie, C. Chen, A. Weston, N. Miura, L. Sorokin, R. Adams, A.F. Muro, D. Sheppard, and T. Makinen. 2009. Integrin-alpha9 is required for fibronectin matrix assembly during lymphatic valve morphogenesis. *Dev. Cell*. 17:175–186. http://dx.doi.org/10.1016/j.devcel.2009.06.017

Chai, X., E. Förster, S. Zhao, H.H. Bock, and M. Frotscher. 2009. Reelin stabilizes the actin cytoskeleton of neuronal processes by inducing n-cofilin phosphorylation at serine3. *J. Neurosci.* 29:288–299. http://dx.doi.org/10.1523/JNEUROSCI.2934-08.2009

D'Arcangelo, G., G.G. Miao, S.C. Chen, H.D. Soares, J.I. Morgan, and T. Curran. 1995. A protein related to extracellular matrix proteins deleted in the mouse mutant reeler. *Nature*. 374:719–723. http://dx.doi.org/10.1038/374719a0

Figueroa, J.E., J. Oubre, and P. Vijayagopal. 2004. Modulation of vascular smooth muscle cells proteoglycan synthesis by the extracellular matrix. *J. Cell. Physiol.* 198:302–309. http://dx.doi.org/10.1002/jcp.10414

Franco, S.J., I. Martinez-Garay, C. Gil-Sanz, S.R. Harkins-Perry, and U. Müller. 2011. Reelin regulates cadherin function via Dab1/Rap1 to control neuronal migration and lamination in the neocortex. *Neuron*. 69:482–497. http://dx.doi.org/10.1016/j.neuron.2011.01.003

Frykman, P.K., M.S. Brown, T. Yamamoto, J.L. Goldstein, and J. Herz. 1995. Normal plasma lipoproteins and fertility in gene-targeted mice homozygous for a disruption in the gene encoding very low density lipoprotein receptor. *Proc. Natl. Acad. Sci. USA*. 92:8453–8457. http://dx.doi.org/10.1073/pnas.92.18.8453

Gentleman, R.C., V.J. Carey, D.M. Bates, B. Bolstad, M. Dettling, S. Dudoit, B. Ellis, L. Gautier, Y. Ge, J. Gentry, et al. 2004. Bioconductor: open software development for computational biology and bioinformatics. *Genome Biol.* 5:R80. http://dx.doi.org/10.1186/gb-2004-5-10-r80

Hack, I., S. Hellwig, D. Junghans, B. Brunne, H.H. Bock, S. Zhao, and M. Frotscher. 2007. Divergent roles of ApoER2 and Vldlr in the migration of cortical neurons. *Development*. 134:3883–3891. http://dx.doi.org/10.1242/dev.005447

Hartfuss, E., E. Förster, H.H. Bock, M.A. Hack, P. Leprince, J.M. Luque, J. Herz, M. Frotscher, and M. Götz. 2003. Reelin signaling directly affects radial glia morphology and biochemical maturation. *Development*. 130:4597–4609. http://dx.doi.org/10.1242/dev.00654

Hellström, M., H. Gerhardt, M. Kalén, X. Li, U. Eriksson, H. Wolburg, and C. Betsholtz. 2001. Lack of pericytes leads to endothelial hyperplasia and abnormal vascular morphogenesis. *J. Cell Biol.* 153:543–553. http://dx.doi.org/10.1083/jcb.153.3.543

Hong, S.E., Y.Y. Shugart, D.T. Huang, S.A. Shahwan, P.E. Grant, J.O. Hourihane, N.D. Martin, and C.A. Walsh. 2000. Autosomal recessive lissencephaly with cerebellar hypoplasia is associated with human RELN mutations. *Nat. Genet.* 26:93–96. http://dx.doi.org/10.1038/79246

Hynes, R.O. 2009. The extracellular matrix: not just pretty fibrils. *Science*. 326:1216–1219. http://dx.doi.org/10.1126/science.1176009

Irizarry, R.A., B.M. Bolstad, F. Collin, L.M. Cope, B. Hobbs, and T.P. Speed. 2003. Summaries of Affymetrix GeneChip probe level data. *Nucleic Acids Res.* 31:e15. http://dx.doi.org/10.1093/nar/gng015

Jossin, Y., L. Gui, and A.M. Goffinet. 2007. Processing of Reelin by embryonic neurons is important for function in tissue but not in dissociated cultured neurons. *J. Neurosci.* 27:4243–4252. http://dx.doi.org/10.1523/JNEUROSCI.0023-07.2007

Jurisic, G., and M. Detmar. 2009. Lymphatic endothelium in health and disease. *Cell Tissue Res.* 335:97–108. http://dx.doi.org/10.1007/s00441-008-0644-2

Kalluri, R. 2003. Basement membranes: structure, assembly and role in tumour angiogenesis. *Nat. Rev. Cancer*. 3:422–433. http://dx.doi.org/10.1038/nrc1094

Kärpänen, T., C.A. Heckman, S. Keskitalo, M. Jeltsch, H. Ollila, G. Neufeld, L. Tamagnone, and K. Alitalo. 2006. Functional interaction of VEGF-C and VEGF-D with neuropilin receptors. *FASEB J.* 20:1462–1472. http://dx.doi.org/10.1096/fj.05-5646com

Keilani, S., and K. Sugaya. 2008. Reelin induces a radial glial phenotype in human neural progenitor cells by activation of Notch-1. *BMC Dev. Biol.* 8:69. http://dx.doi.org/10.1186/1471-213X-8-69

Kubo, K., K. Mikoshiba, and K. Nakajima. 2002. Secreted Reelin molecules form homodimers. *Neurosci. Res.* 43:381–388. http://dx.doi.org/10.1016/S0168-0102(02)00068-8

Lambert de Rouvroit, C., V. de Bergeyck, C. Cortvrindt, I. Bar, Y. Eeckhout, and A.M. Goffinet. 1999. Reelin, the extracellular matrix protein deficient in reeler mutant mice, is processed by a metalloproteinase. *Exp. Neurol.* 156:214–217. http://dx.doi.org/10.1006/exnr.1998.7007

Ma, G.C., C.S. Liu, S.P. Chang, K.T. Yeh, Y.Y. Ke, T.H. Chen, B.B. Wang, S.J. Kuo, J.C. Shih, and M. Chen. 2008. A recurrent ITGA9 missense mutation in human fetuses with severe chylothorax: possible correlation with poor response to fetal therapy. *Prenat. Diagn.* 28:1057–1063. http://dx.doi.org/10.1002/pd.2130

Mäkinen, T., T. Veikkola, S. Mustjoki, T. Karpanen, B. Catimel, E.C. Nice, L. Wise, A. Mercer, H. Kowalski, D. Kerjaschki, et al. 2001. Isolated lymphatic endothelial cells transduce growth, survival and migratory signals via the VEGF-C/D receptor VEGFR-3. *EMBO J.* 20:4762–4773. http://dx.doi.org/10.1093/emboj/20.17.4762

Mäkinen, T., R.H. Adams, J. Bailey, Q. Lu, A. Ziemiecki, K. Alitalo, R. Klein, and G.A. Wilkinson. 2005. PDZ interaction site in ephrinB2 is required for the remodeling of lymphatic vasculature. *Genes Dev.* 19:397–410. http://dx.doi.org/10.1101/gad.330105

Ogawa, M., T. Miyata, K. Nakajima, K. Yagyu, M. Seike, K. Ikenaka, H. Yamamoto, and K. Mikoshiba. 1995. The reeler gene-associated antigen on Cajal-Retzius neurons is a crucial molecule for laminar organization of cortical neurons. *Neuron*. 14:899–912. http://dx.doi.org/10.1016/0896-6273(95)90329-1

Pflicke, H., and M. Sixt. 2009. Preformed portals facilitate dendritic cell entry into afferent lymphatic vessels. *J. Exp. Med.* 206:2925–2935. http://dx.doi.org/10.1084/jem.20091739

Religa, P., R. Cao, M. Bjorndahl, Z. Zhou, Z. Zhu, and Y. Cao. 2005. Presence of bone marrow-derived circulating progenitor endothelial cells in the newly formed lymphatic vessels. *Blood*. 106:4184–4190. http://dx.doi.org/10.1182/blood-2005-01-0226

Ringelmann, B., C. Röder, R. Hallmann, M. Maley, M. Davies, M. Grounds, and L. Sorokin. 1999. Expression of laminin alpha1, alpha2, alpha4, and alpha5 chains, fibronectin, and tenascin-C in skeletal muscle of dystrophic 129ReJ dy/dy mice. *Exp. Cell Res.* 246:165–182. http://dx.doi.org/10.1006/excr.1998.4244

Samama, B., and N. Boehm. 2005. Reelin immunoreactivity in lymphatics and liver during development and adult life. *Anat. Rec. A Discov. Mol. Cell. Evol. Biol.* 285:595–599.

Sasaki, T., R. Fässler, and E. Hohenester. 2004. Laminin: the crux of basement membrane assembly. *J. Cell Biol.* 164:959–963. http://dx.doi.org/10.1083/jcb.200401058

Scallan, J.P., and V.H. Huxley. 2010. In vivo determination of collecting lymphatic vessel permeability to albumin: a role for lymphatics in exchange. *J. Physiol.* 588:243–254. http://dx.doi.org/10.1113/jphysiol.2009.179622

Stenzel, D., E. Nye, M. Nisancioglu, R.H. Adams, Y. Yamaguchi, and H. Gerhardt. 2009. Peripheral mural cell recruitment requires cell-autonomous heparan sulfate. *Blood*. 114:915–924. http://dx.doi.org/10.1182/blood-2008-10-186239

Tammela, T., and K. Alitalo. 2010. Lymphangiogenesis: Molecular mechanisms and future promise. *Cell*. 140:460–476. http://dx.doi.org/10.1016/j.cell.2010.01.045

Tinnes, S., M.K. Schäfer, A. Flubacher, G. Münzner, M. Frotscher, and C.A. Haas. 2011. Epileptiform activity interferes with proteolytic processing of Reelin required for dentate granule cell positioning. *FASEB J.* 25:1002–1013. http://dx.doi.org/10.1096/fj.10-168294

Tissir, F., and A.M. Goffinet. 2003. Reelin and brain development. *Nat. Rev. Neurosci.* 4:496–505. http://dx.doi.org/10.1038/nrn1113

Trommsdorff, M., M. Gotthardt, T. Hiesberger, J. Shelton, W. Stockinger, J. Nimpf, R.E. Hammer, J.A. Richardson, and J. Herz. 1999. Reeler/Disabled-like disruption of neuronal migration in knockout mice lacking the VLDL receptor and ApoE receptor 2. *Cell*. 97:689–701. http://dx.doi.org/10.1016/S0092-8674(00)80782-5

Utsunomiya-Tate, N., K. Kubo, S. Tate, M. Kainosho, E. Katayama, K. Nakajima, and K. Mikoshiba. 2000. Reelin molecules assemble together to form a large protein complex, which is inhibited by the function-blocking CR-50 antibody. *Proc. Natl. Acad. Sci. USA*. 97:9729–9734. http://dx.doi.org/10.1073/pnas.160272497

Veikkola, T., M. Lohela, K. Ikenberg, T. Mäkinen, T. Korff, A. Saaristo, T. Petrova, M. Jeltsch, H.G. Augustin, and K. Alitalo. 2003. Intrinsic versus microenvironmental regulation of lymphatic endothelial cell phenotype and function. *FASEB J.* 17:2006–2013. http://dx.doi.org/10.1096/fj.03-0179com

von der Weid, P.Y., and D.C. Zawieja. 2004. Lymphatic smooth muscle: the motor unit of lymph drainage. *Int. J. Biochem. Cell Biol.* 36:1147–1153. http://dx.doi.org/10.1016/j.biocel.2003.12.008

Wang, W., Z. Nepiyushchikh, D.C. Zawieja, S. Chakraborty, S.D. Zawieja, A.A. Gashev, M.J. Davis, and M. Muthuchamy. 2009. Inhibition of myosin light chain phosphorylation decreases rat mesenteric lymphatic contractile activity. *Am. J. Physiol. Heart Circ. Physiol.* 297:H726–H734. http://dx.doi.org/10.1152/ajpheart.00312.2009

Wu, C., F. Ivars, P. Anderson, R. Hallmann, D. Vestweber, P. Nilsson, H. Robenek, K. Tryggvason, J. Song, E. Korpos, et al. 2009. Endothelial basement membrane laminin alpha5 selectively inhibits T lymphocyte extravasation into the brain. *Nat. Med.* 15:519–527. http://dx.doi.org/10.1038/nm.1957

Zhao, S., and M. Frotscher. 2010. Go or stop? Divergent roles of Reelin in radial neuronal migration. *Neuroscientist*. 16:421–434. http://dx.doi.org/10.1177/1073858410367521